Supplement of Atmos. Chem. Phys., 25, 1569–1585, 2025
https://doi.org/10.5194/acp-25-1569-2025-supplement

Atmospheric Chemistry and Physics
Open Access

Supplement of

Impacts of meteorology and emission reductions on haze pollution during the lockdown in the North China Plain

Lang Liu et al.

Correspondence to: Xin Long (longxin@cigit.ac.cn) and Yi Li (liyiqxxy@163.com)

S1. Statistical methods for comparisons

We assessed the model performance using several statistical parameters, including normalized mean bias (*NMB*), index of agreement (*IOA*), and correlation coefficient (*r*), to compare simulations against observational data. The evaluated variables encompass air pollutants such as $PM_{2.5}$, O_3, NO_2, SO_2, and CO concentrations within the NNCP and SNCP regions. $PM_{2.5}$ components, including organic, nitrate, sulfate, and ammonium, are also assessed at the IAP monitoring site. These statistical metrics provide a quantitative measure of how well the model reproduces the observed data, offering insights into its accuracy and reliability in simulating the atmospheric conditions and pollutant levels during the specified period.

$$NMB = \frac{\sum_{i=1}^{N}(P_i - O_i)}{\sum_{i=1}^{N} O_i} \quad \text{(S1)}$$

$$IOA = 1 - \frac{\sum_{i=1}^{N}(P_i - O_i)^2}{\sum_{i=1}^{N}(|P_i - \overline{O}| + |O_i - \overline{O}|)^2} \quad \text{(S2)}$$

$$r = \frac{\sum_{i=1}^{N}(P_i - \overline{P})(O_i - \overline{O})}{\left[\sum_{i=1}^{N}(P_i - \overline{P})^2 \sum_{i=1}^{N}(O_i - \overline{O})^2\right]^{\frac{1}{2}}} \quad \text{(S3)}$$

where P_i and O_i represent the calculated and observed variables, respectively. N stands for the total number of predictions for comparison, and $\overline{O}$ and $\overline{P}$ denote the average observations and simulations, respectively. The *IOA* ranges from 0 to 1, where a value of 1 indicates perfect agreement between the predictions and observations. The *r* ranges from -1 to 1, 1 indicating perfect spatial consistency between the observations and predictions.

S2. Mean meteorlogy over 2015 to 2019

This study's mean meteorology field data was derived by averaging key meteorological variables (e.g., temperature, wind speed, relative humidity, and pressure) from 2015 to 2019. Given that the vertical levels in the NCEP FNL data varied across different years, we did not average the original data directly. Instead, we processed the data using the WRF Preprocessing System (WPS) to ensure consistency. Specifically, we ran WPS for each year to generate the met_em* files containing processed meteorological variables at uniform vertical levels and grid resolution. We then averaged these met_em* files across the six years at each grid point and pressure level, which helped preserve the atmospheric variables' vertical structure and physical coherence. This approach maintained a realistic representation of the atmospheric state by accounting for the multi-year variability while ensuring that the averaged fields were consistent with the WRF-Chem grid resolution. As the WPS processing already matched the data to the model's spatial resolution, no additional interpolation was required, thus ensuring the physical and spatial consistency of the averaged

climatological fields used in the WRF-Chem simulations. This multi-year climatological averaging was designed to capture the typical variations in initial and boundary meteorological conditions. This approach provided a robust and representative baseline for multiple years, effectively minimizing the influence of anomalies or extreme weather events characteristic of any individual year.

S3. Factor separation technique to analyze coupled effects

In nonlinear atmospheric systems, factors often interact in complex ways, making it hard to identify their individual impacts. To address this, we used the factor separation approach (FSA) by Stein and Alpert (1993), which helps separate the direct effects of each factor from their interactions. In this study, we focused on emissions and meteorological changes, aiming to understand both their individual effects and how they interact. The pure contributions from emission reductions and meteorological changes are represented as follows:

$$f'_{EMIS} = f_{EMIS} - f_{BASE} \quad \text{(S4)}$$

$$f'_{METEO} = f_{METEO} - f_{BASE} \quad \text{(S5)}$$

When emissions and meteorological conditions are considered, the total impact includes their individual contributions and coupled. The combined effect is expressed as:

$$f_{EMIS\_METEO} = f'_{EMIS} + f'_{METEO} + f'_{EMIS\_METEO} + f_{BASE} \quad \text{(S6)}$$

To quantify the coupled effects between emissions and meteorological changes, we use the following equation:

$$\begin{aligned} f'_{EMIS\_METEO} &= f_{EMIS\_METEO} - f'_{EMIS} - f'_{METEO} - f_{BASE} \\ &= f_{EMIS\_METEO} - (f_{EMIS} - f_{BASE}) - (f_{METEO} - f_{BASE}) - f_{BASE} \\ &= f_{EMIS\_METEO} - f_{EMIS} - f_{METEO} + f_{BASE} \end{aligned} \quad \text{(S7)}$$

This final form helps us understand how the combined effects relate to individual impacts and the baseline. Using the FSA, we can clearly see how emissions and meteorological conditions contribute to changes in the atmosphere.

Figure S1

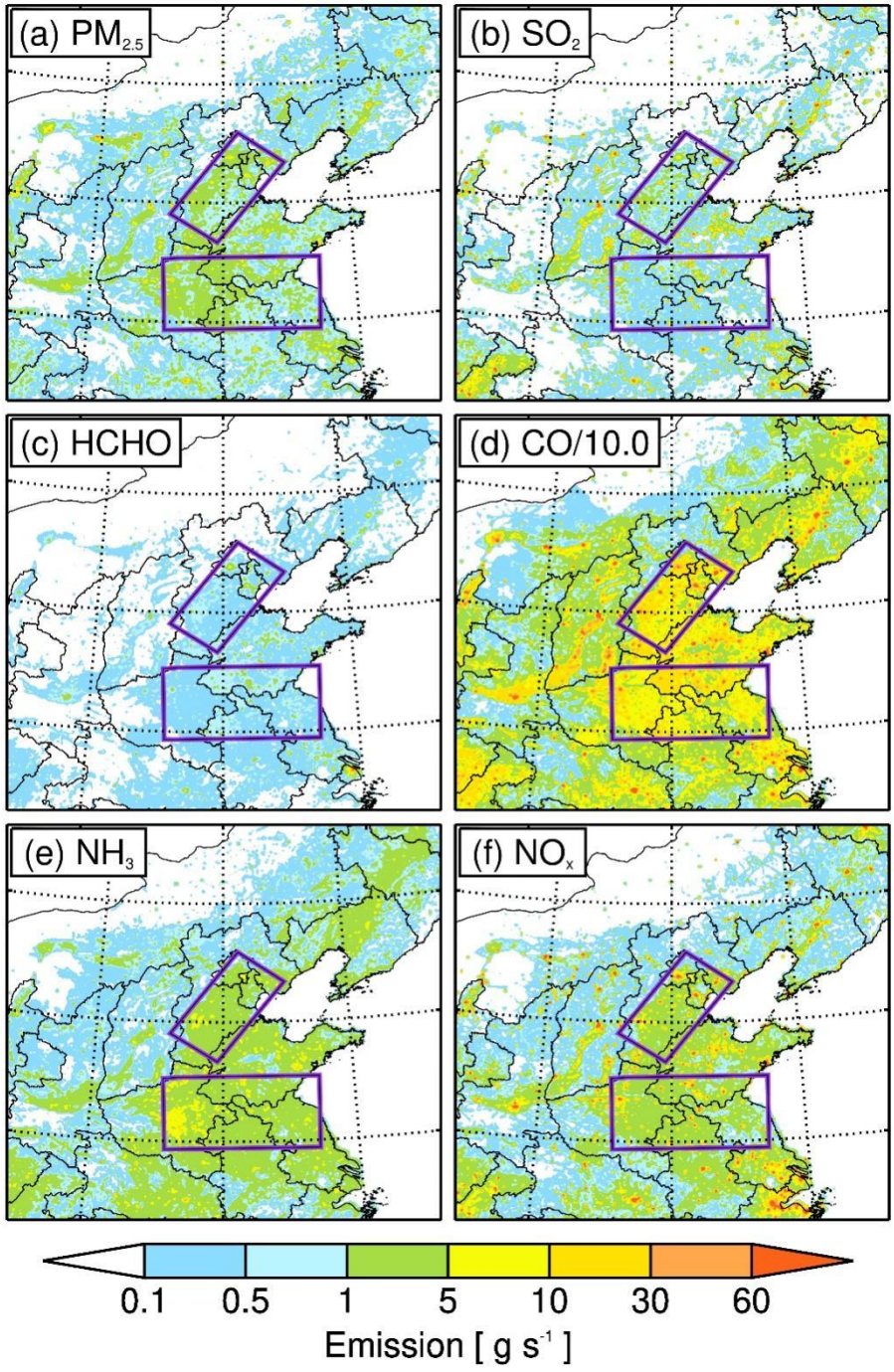

Figure S1 Spatial distributions of pollutants in the research domain during the COVID-19 lockdown. (a) $PM_{2.5}$, (b) SO_2, (c) HCHO, (d) CO, (e) NH_3, and (f) NO_x. SO_2, NO_x, NH_3, and HCHO (an effective indicator for VOCs) are gaseous precursors for secondary aerosols in $PM_{2.5}$. The regions of interest, NNCP (Northern North China Plain) and SNCP (Southern North China Plain), are highlighted.

Figure S2

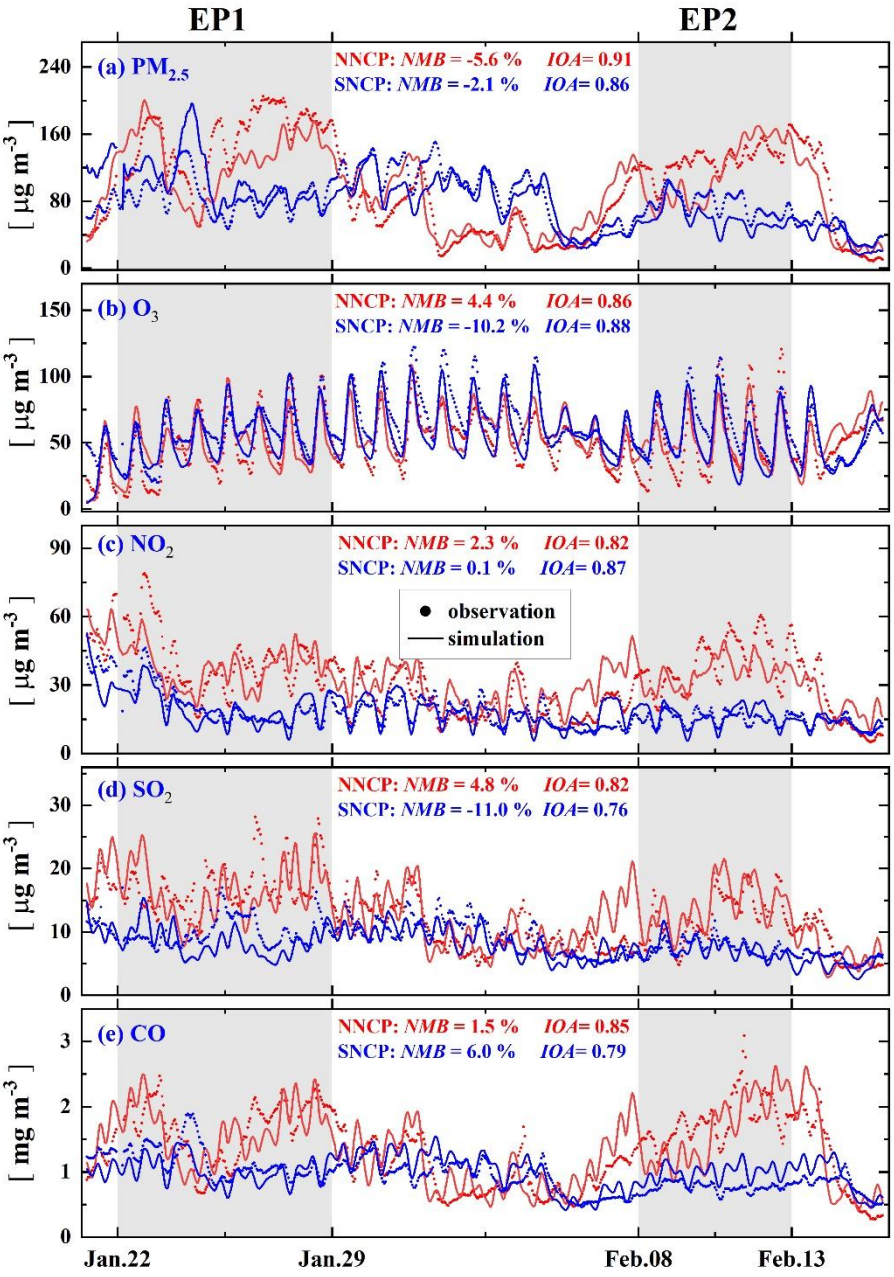

Figure S2. Comparisons of simulated and observed near-surface mass concentrations of (a) $PM_{2.5}$, (b) O_3, (c) NO_2, (d) SO_2, and (e) CO averaged across all ambient monitoring stations in the NNCP (red) and SNCP (blue) from 21 January to 16 February 2020. Solid lines represent simulated concentrations, while dots indicate observed concentrations.

Figure S3

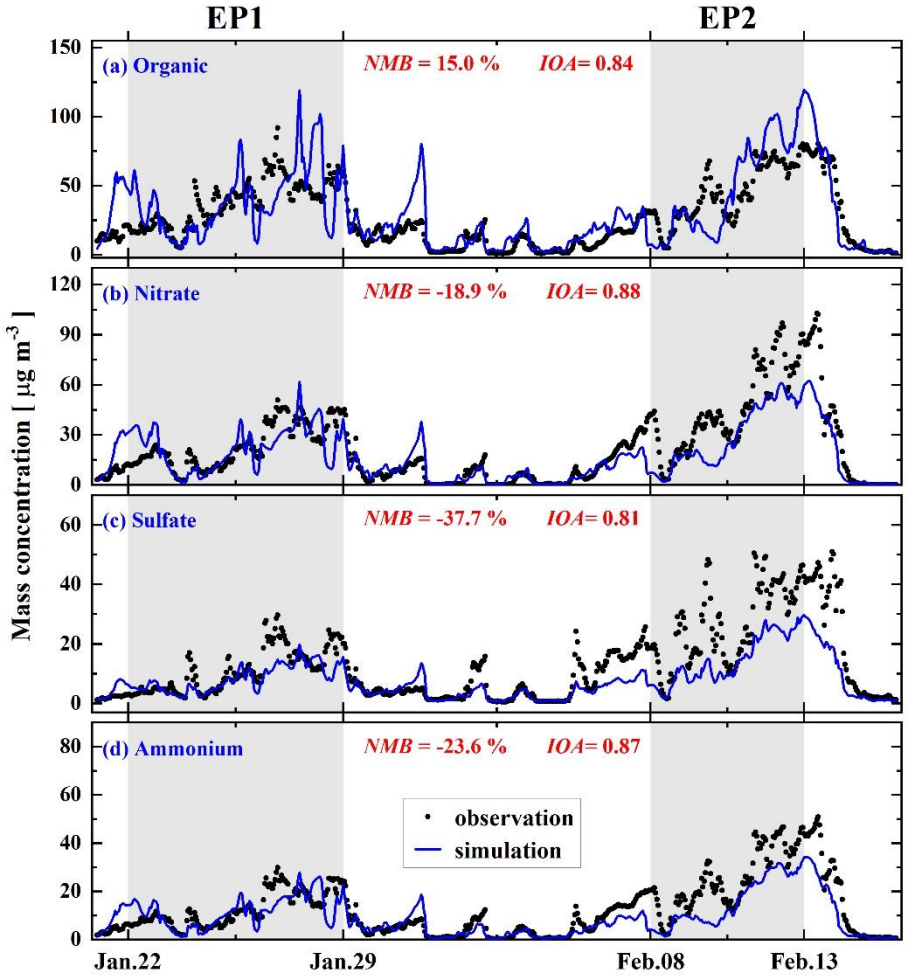

Figure S3. Comparisons of simulated and observed mass concentrations of (a) organic, (b) nitrate, (c) sulfate, and (d) ammonium at the IAP monitoring site from 21 January to 16 February 2020. Blue lines represent simulated concentrations, while black dots indicate observed concentrations.

Figure S4

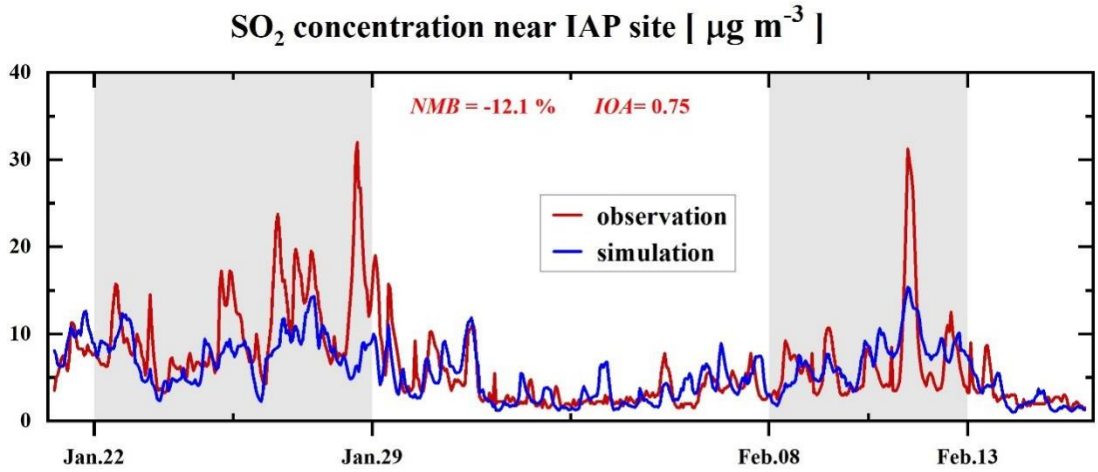

Figure S4. Comparisons of simulated and observed mass concentrations of SO_2 near the IAP site monitoring site from 21 January to 16 February 2020. Blue lines represent simulated concentrations, while red lines indicate observed concentrations.

Figure S5

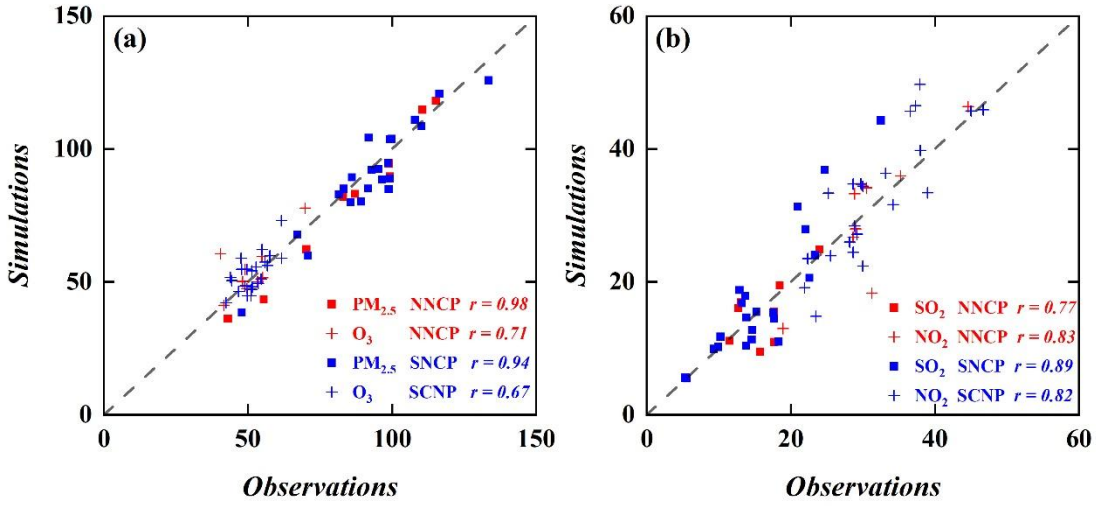

Figure S5. Statistical comparisons of model simulations and observations for (a) $PM_{2.5}$ and O_3, and (b) SO_2 and NO_2 in the NNCP and SNCP regions.

Figure S6

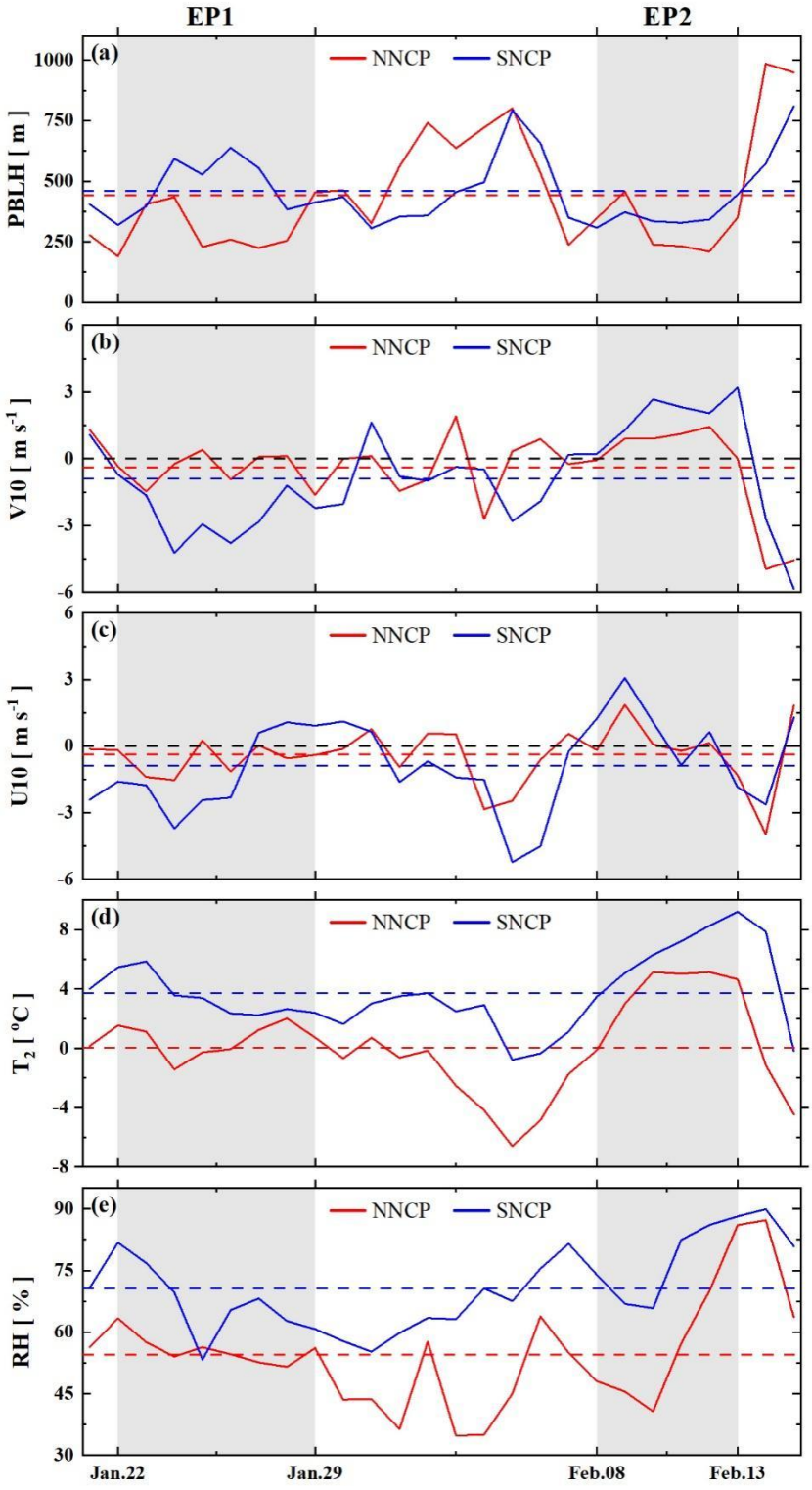

Figure S6. Regional day-to-day variations in (a) PBLH, (b) V10, (c) U10, (d) V10, and (e) RH in the NNCP and SNCP from 21 January to 16 February 2020.

Figure S7

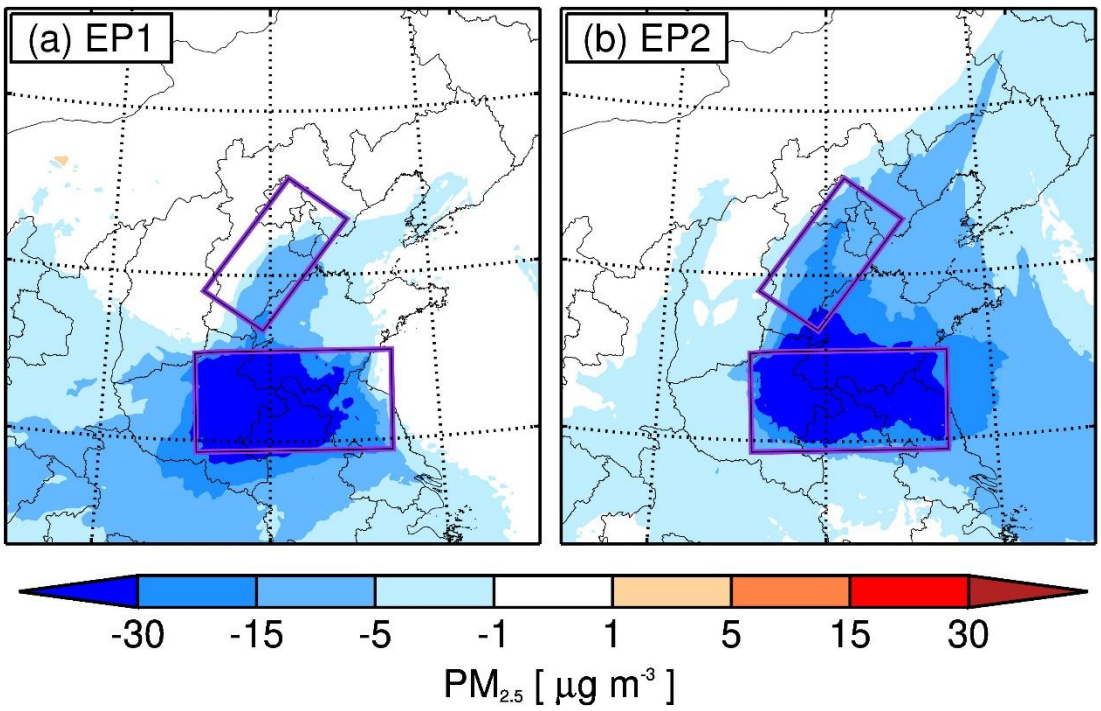

Figure S7. The pattern comparisons of "SNCP0" simulations minus the "BASE" simulation. The color gradient represents $PM_{2.5}$ changes averaged from (a) the EP1 haze period, and (b) the EP2 haze period,

Figure S8

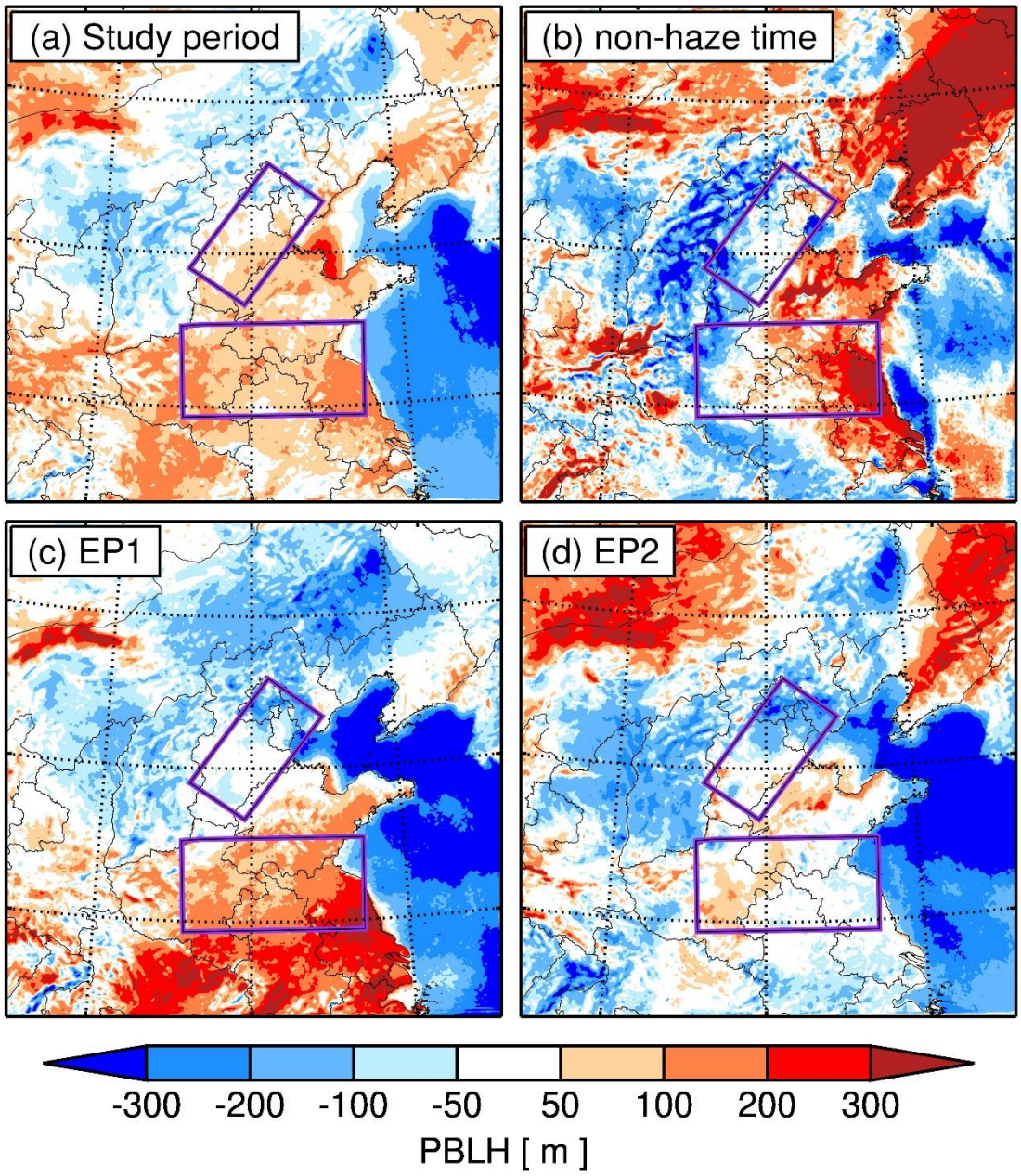

Figure S8. The pattern comparisons of the "BASE" simulation minus the "METEO" simulation. The color gradient represents PBLH changes averaged from (a) the entire study period, (b) the non-haze period, (c) the EP1 haze period, and (d) the EP2 haze period.

Figure S9

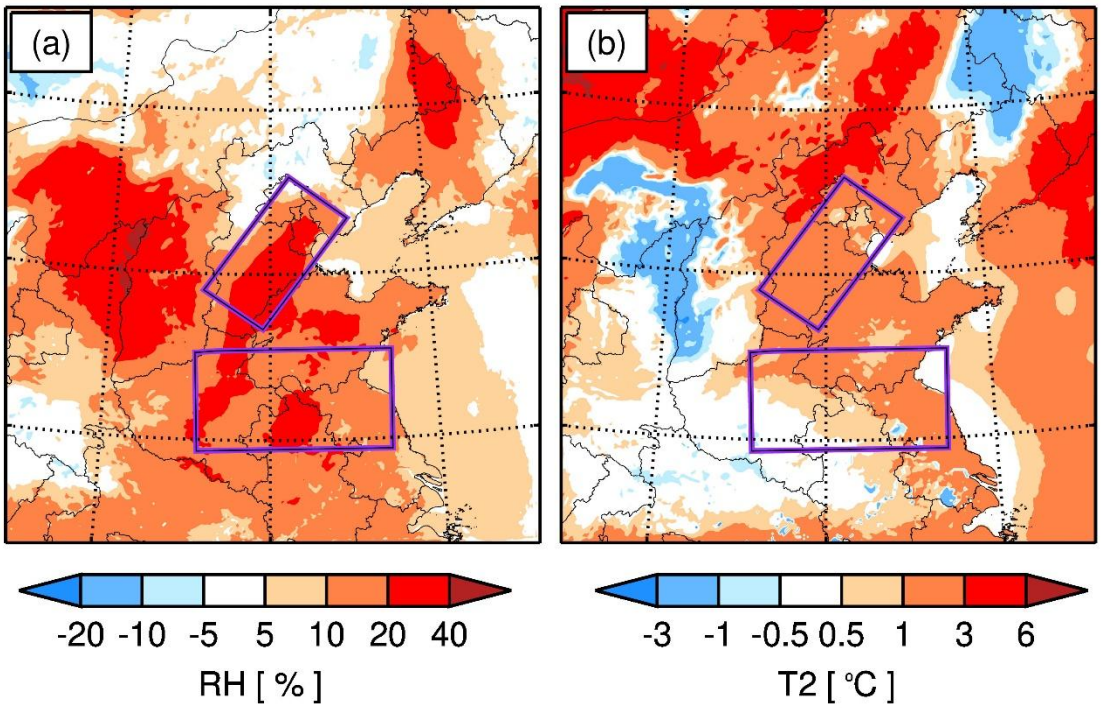

Figure S9. The pattern comparisons between the "BASE" and "SEN_METEO" simulations. The color gradient represents (a) relative humidity (RH) changes and (b) near-surface temperature (T_2) changes averaged from the study period.

Figure S10

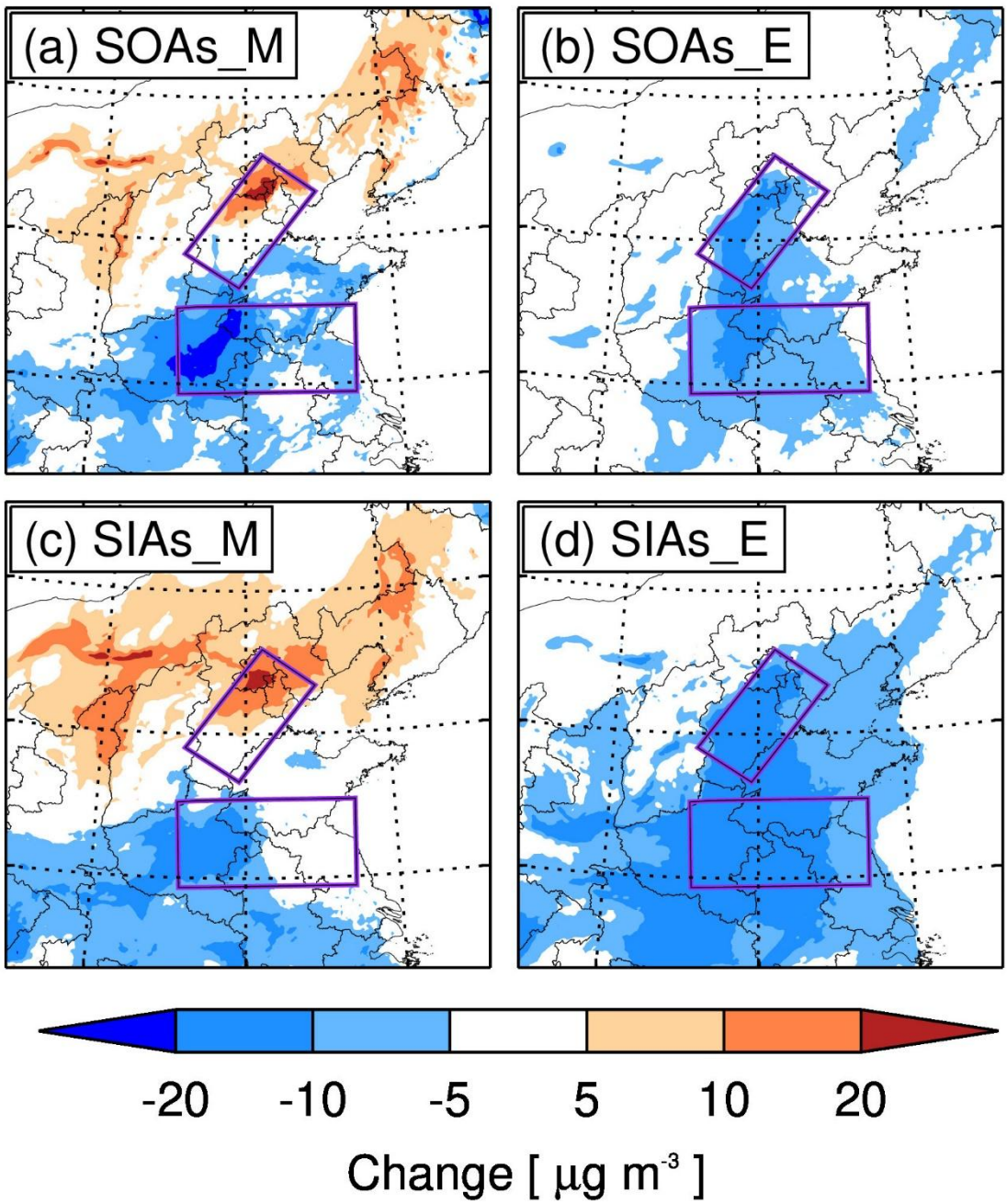

Figure S10. Comparison of simulated changes in chemical components during the study period between the "BASE" scenario and two sensitivity cases: (a,c) " METEO" and (b,d) "EMIS". The chemical components include (a,c) secondary organic aerosols and (b,d) secondary inorganic aerosols (SIAs), including sulfate, nitrate, and ammonium.

Figure S11

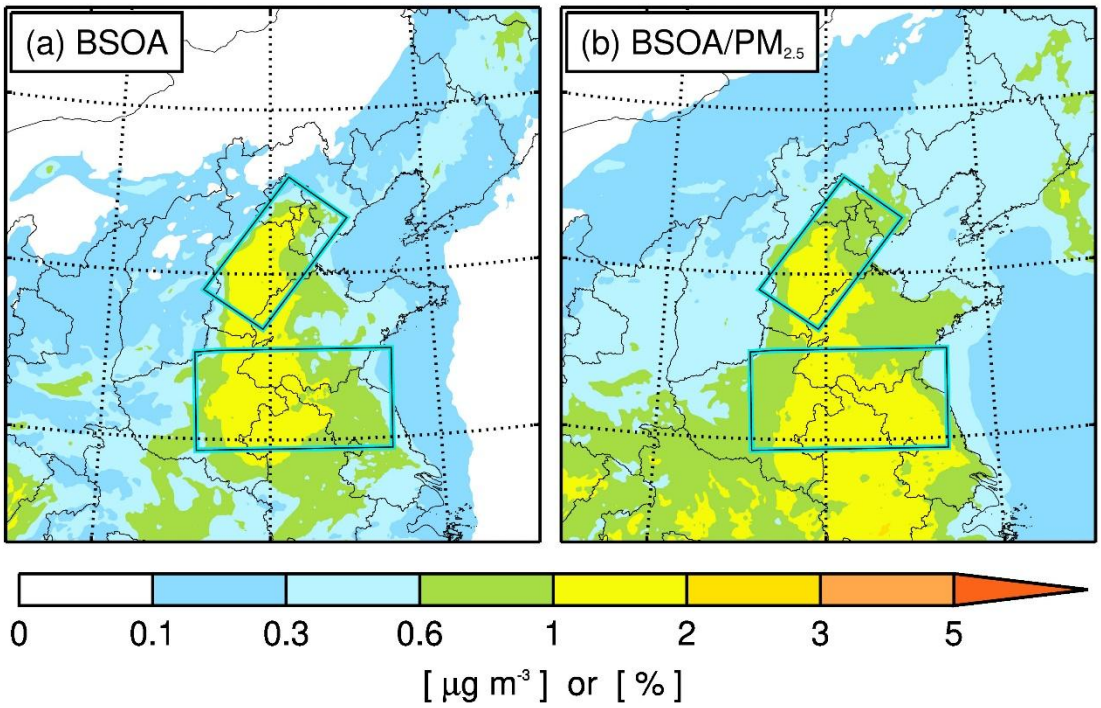

Figure S11. Spatial distribution of (a) near-surface biogenic SOA mass concentration and (b) its contribution as a percentage of $PM_{2.5}$ in the BASE simulations over the study period.

Figure S12

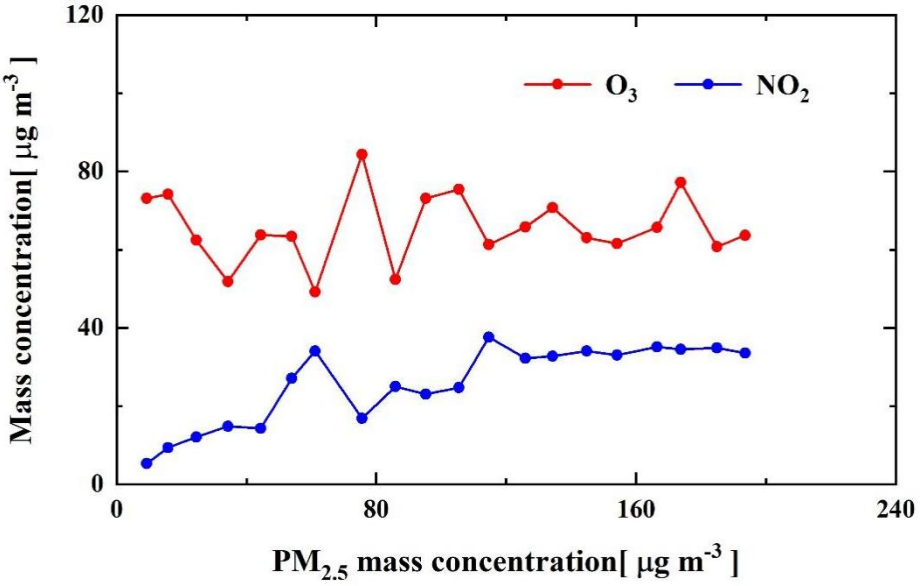

Figure S12. Daytime variation of O_3 and NO_2 (10:00 to 16:00 Beijing Time) as a function of $PM_{2.5}$ concentration during the study period in the NNCP.

Figure S13

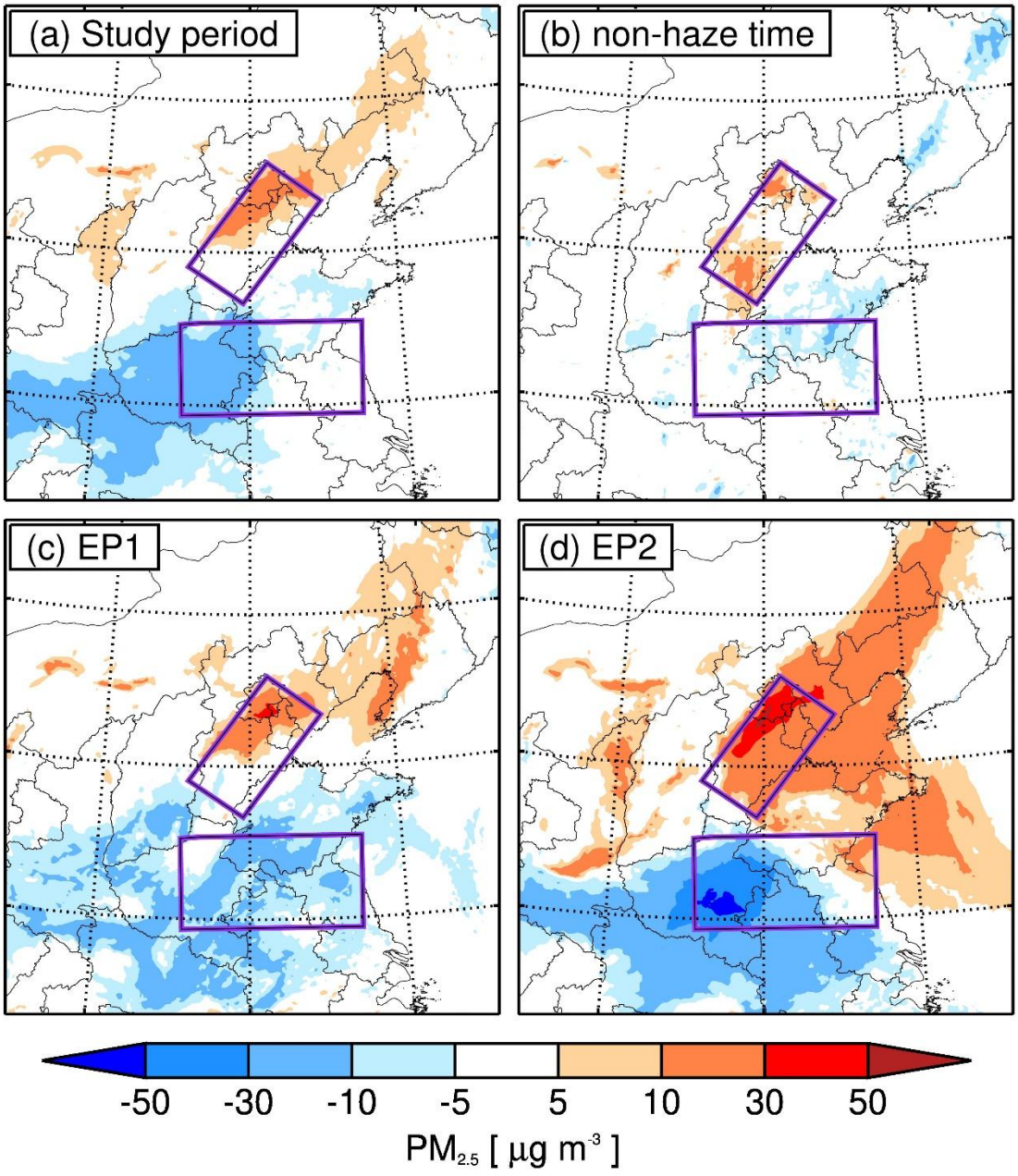

Figure S13. The coupled effects between emission reductions and meteorological factors on $PM_{2.5}$. The color gradient coupled effects averaged from (a) the entire study period, (b) the non-haze period, (c) the EP1 haze period, and (d) the EP2 haze period.

Figure S14

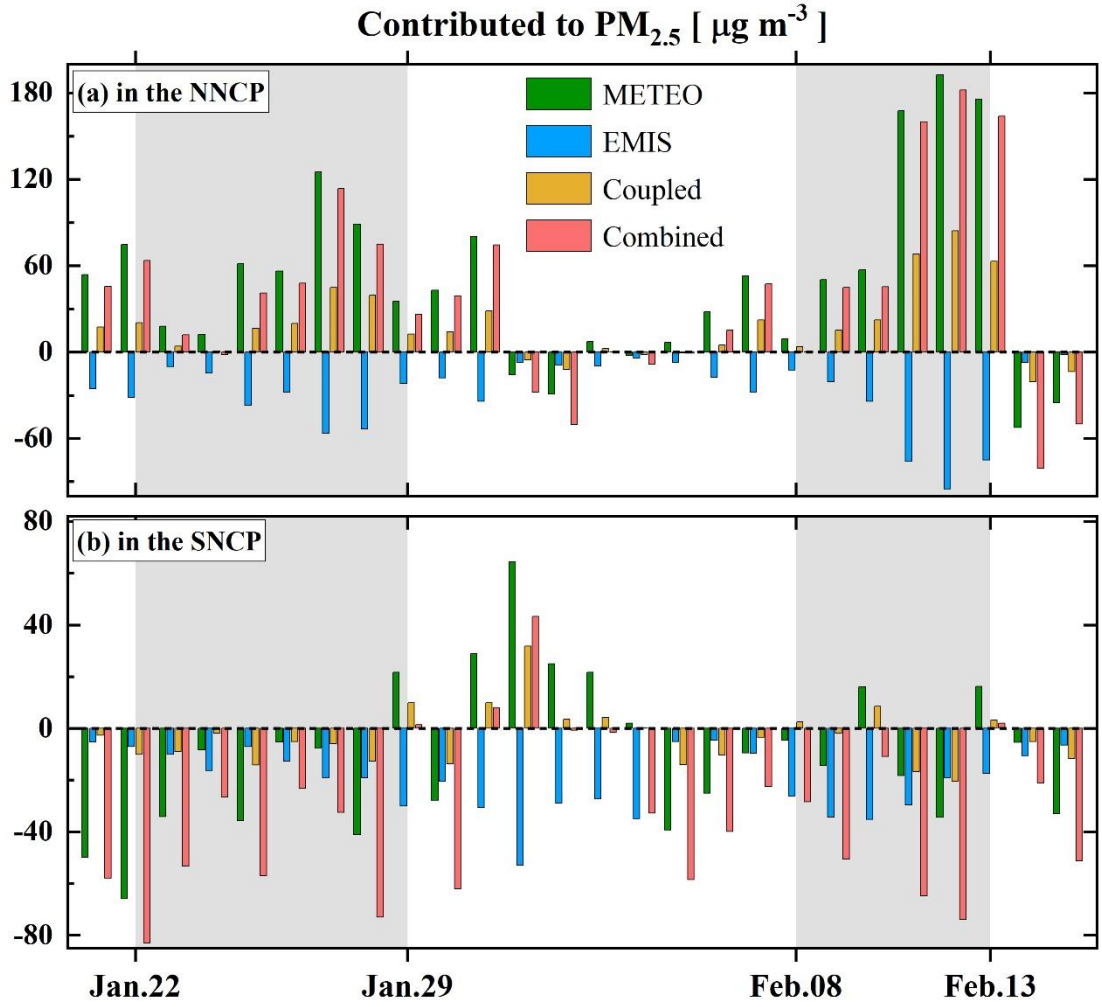

Figure S14. Regional contributions to daily $PM_{2.5}$ averaged in (a) the NNCP and (b) the SNCP. The contributions include meteorological conditions (METEO), abrupt anthropogenic emissions (EMIS) decreases, and coupled and combined effects of METEO and EMIS.

Table S1 Model configuration for the simulation domain, meteorological schemes, chemical mechanisms, initial and lateral conditions, and emission inventories.

Domain	
Size	300 × 300 horizontal grid cells
Center	116°E, 38° N
Horizontal resolution	6 km × 6 km
Vertical resolution	35 vertical levels, uneven intervals, spacing ranging from ~50 m near the surface, ~500 m at 2.5 km above the ground level, and more than 1 km at 14 km above the ground level
Meteorology	
Microphysics scheme	WSM 6-class graupel microphysics scheme (Hong and Lim, 2006)
Boundary layer scheme	MYJ PBL scheme (Janjić, 2002)
Surface layer scheme	Monin-Obukhov surface layer scheme (Janjić, 2002)
Land-surface scheme	Noah land-surface model (Chen and Dudhia, 2001)
Longwave radiation scheme	Goddard (Dudhia, 1989)
Shortwave radiation scheme	Goddard (Dudhia, 1989)
Dry deposition	Wesely (1989)
Wet deposition	CMAQ (Binkowski and Roselle, 2003)
Chemistry	
Gas phase chemistry	SAPRC99 chemical mechanism (Binkowski and Roselle, 2003)
Inorganic aerosols	ISORROPIA version 1.7 (Nenes et al., 1998)
Secondary organic aerosol	Nontraditional VBS parametrization (Li et al., 2011)
Photolysis rates	FTUV radiation transfer model (Tie et al., 2003)
Boundary and initial conditions	
Meteorological	NCEP FNL 6-hr 1° × 1° analysis data
Chemical	CAM-chem 6-hr outputs
Emission inventory	
Anthropogenic	MEIC (Zhang et al. 2009; Li et al., 2017)
Biogenic	MEGAN (Guenther et al., 2006)

Table S2 Provincial emission reduction ratios during the COVID-19 lockdown period in 2020 in the study area.

Species / Province	CO	NO_x	SO_2	VOCs	$PM_{2.5}$	BC	OC
Beijing	22%	45%	26%	45%	18%	46%	8%
Tianjin	21%	38%	20%	41%	14%	22%	6%
Hebei	15%	45%	16%	36%	12%	17%	5%
Anhui	14%	56%	22%	31%	11%	22%	4%
Inner Mongolia	14%	29%	15%	34%	13%	16%	6%
Shaanxi	19%	45%	18%	34%	13%	22%	5%
Hubei	19%	55%	23%	35%	16%	23%	10%
Jilin	16%	39%	23%	34%	13%	18%	5%
Liaoning	21%	40%	28%	36%	16%	28%	8%
Henan	23%	57%	22%	41%	18%	35%	8%
Shandong	23%	50%	25%	39%	19%	35%	9%
Jiangsu	23%	50%	26%	41%	16%	35%	7%
Shanghai	35%	48%	42%	45%	34%	54%	42%